Available online at www.sciencedirect.com

SciVerse ScienceDirect

Ceramics International 39 (2013) S153–S158

CERAMICS INTERNATIONAL

www.elsevier.com/locate/ceramint

Multi-physics analysis on a unimorphic piezoelectric diaphragm according to its shape and boundary conditions for the performance enhancement

Sungjoon Choi[a], Youngtaek Cha[a], Jongkyu Park[b,*], Hongseok Jang[b]

[a]Korea Institute of Industrial Technology (KITECH), 8F, Daegu Convergence R&D Center, 711, Hosan-dong, Dalseo-gu, Daegu 704–230, South Korea
[b]Department of Mechanical Engineering, Changwon National University Room 53301, #9 Sarim-dong, Changwon, Gyeongnam 641–773, South Korea

Available online 23 October 2012

Abstract

A micro-viscometer for measuring viscosity change in small amount of liquid in real time has been proposed recently. The advantages of the device are the use of minimal liquid and maximized sensitivity for measuring viscosity. However, in previous research, even though the multi-physical simulation including electrical, mechanical, and acoustical phenomenon is necessary for design of micro-viscometer, only acoustical aspects have been considered. Thus, combined physical phenomena could not be reflected for an optimum design process. In this research, a multi-physical approach is developed for designing a micro-viscometer, and an optimized micro-viscometer design is proposed. The proposed method is able to capture multi-physical phenomena such as near field effect and added mass effect. It also has the advantage of flexible design of various shape and materials, leading to savings of cost and time.

Keywords: Micorochannel; Micro-viscometer; Wave attenuation; MEMS

1. Introduction

Recently, a micro-viscometer was proposed to measure the viscosity variation of minimal liquid (13 nl) using the propagation of acoustic waves in microchannels [1]. The micro-viscometer consists of two chambers and four microchannels connecting the two. Each chamber has a unimorphic piezoelectric diaphragm (PZT diaphragm) as a driving and sensing part, as shown in Fig. 1. The sound waves generated from the driving part are propagated to the sensing part through the microchannels and also are attenuated due to viscous effect from the wall of micro-channels. The attenuated sound waves are then transferred to the sensing part, and the output voltage can be measured from the PZT diaphragm of sensing part.

However, only acoustic phenomenon was considered in previously proposed device. The interaction between the Si diaphragm and the internal test liquid, the increase in the stiffness of the Si diaphragm generated from the voltage polarization of PZT diaphragm, and other coupled effects, were not considered in designing previous device. To present an optimized model, multi-physical phenomena including electrical, mechanical, and acoustical phenomenon should be all considered. In this paper, a coupled finite element model is used for multi-physical analysis, and the results are obtained from the proposed method, which has the advantage in designing various shapes and materials, saving cost and time. The proposed method is compared to the previous method in physical aspects [1], and it can be concluded that the coupled finite element model finely captures multi-physical phenomena of the micro-viscometer.

2. Analysis of micro-viscometer simulation

2.1. Multi-physical model of micro-viscometer

Fig. 2 shows a concept of multi-physical micro-viscometer model based on finite element method. Multi-physical model consists of piezoelectric, linear elastic and acoustic body. PZT and Si diaphragm are modeled as

*Corresponding author. Tel.: +82 55 213 3607; fax: +82 55 275 0101.
E-mail address: chong@changwon.ac.kr (J. Park).

0272-8842/$ - see front matter © 2012 Elsevier Ltd and Techna Group S.r.l. All rights reserved.
http://dx.doi.org/10.1016/j.ceramint.2012.10.053

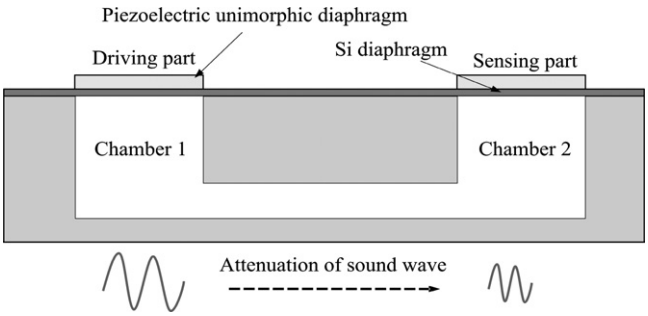

Fig. 1. General shape of micro-viscometer.

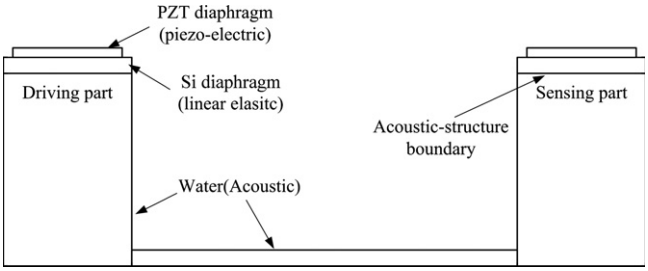

Fig. 2. Multi-physical model of micro-viscometer.

piezoelectric and linear elastic respectively while chambers and channels are modeled as acoustic body filled with water.

This multi-physical model is a combination of piezo-electrical, structural and acoustical phenomenon where each physical quantity is interchanged at its boundaries. For example, when electrical voltage is applied to PZT diaphragm of the driving part, PZT and Si diaphragm of the driving part go under mechanical stress. The mechanical stress then generates structural displacement of PZT–Si diaphragm. The structural displacement of PZT–Si diaphragm acts on boundaries between the PZT–Si diaphragm and the internal water. The displacement creates normal acceleration, or second derivative of the displacement with respect to time, of acoustic pressure on the acoustic-structure boundary. The acceleration generates sound waves that propagate to PZT–Si diaphragm of the sensing part through the microchannels. The propagated sound waves transfer the normal acceleration to the sensing diaphragm. The transferred normal acceleration then reversely causes the structural displacement of PZT–Si diaphragm in the sensing part. Finally, the structural displacement generates electrical voltage on the PZT diaphragm of sensing part.

2.2. Finite element modeling of micro-viscometer

The finite element model used for multi-physical simulation has 44,578 elements with tetra meshes as shown in Fig. 3. The finite element model consists of PZT diaphragm, Si diaphragms, chambers and microchannels. The chamber of driving part is connected to the chamber

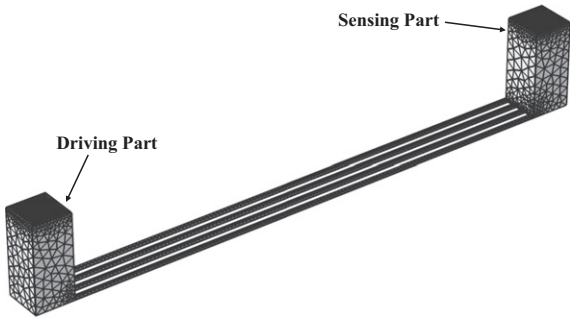

Fig. 3. Finite element model of micro-viscometer.

of the sensing part via four microchannels. The chambers and microchannels are modeled as acoustic fluid with density and sound speed. In order to model the interaction between acoustic medium and structure, the Si diaphragm with linear elastic property is modeled above the chamber. Additionally, the PZT diaphragm, which has piezo-electrical properties based on the stress charge form [2–5], is modeled on top of the Si diaphragm. The detailed properties and dimensions of individual part for the multi-physical simulation are listed in Tables 1 and 2.

In the case of chambers and microchannels, all boundaries except between Si diaphragm and acoustic fluid are set up as rigid wall. The acoustic structure boundary is established as Eq. (1) [6]

$$\alpha_n = \frac{n \cdot \partial^2 u}{\partial t^2} \tag{1}$$

where α_n is a normal acceleration, n is a vector normal to surface of the acoustic structure boundary, and u is structural displacement of PZT–Si diaphragm.

The attenuation coefficient α is applied to water in order to observe the sound attenuation by viscosity of fluid in the microchannels. This attenuation coefficient is calculated by Eq. (2) [7–9].

$$\alpha = \frac{1}{rC_R}\left(\frac{2\pi\eta f}{2\rho_0}\right)^{1/2}\left(1+\frac{\gamma-1}{\sqrt{\mathrm{Pr}}}\right) \tag{2}$$

$$r = \sqrt{\frac{A_{channel}}{\pi}} \tag{3}$$

where $A_{channel}$ is sectional area of the channel, r is equivalent radius for sectional area of the channel, C_R is speed of sound in water, η is shear viscosity coefficient, f is driving frequency, ρ_0 is density of water, γ is ratio of heat capacities and Pr is Prandtl number. The numerical values used in Eq. (2) are listed in Table 3.

The boundary conditions of Si diaphragm and PZT diaphragm are as shown in Figs. 4 and 5. As mentioned earlier Si diaphragm is linear elastic model; hence the fixed displacement condition is applied to the four sides of Si diaphragm while the free displacement condition is applied to top and bottom of the Si diaphragm. In the case of the PZT diaphragm, top of the driving PZT diaphragm is connected to the voltage input and the bottom is grounded

Table 1
Properties of materials.

Material	Property	Value
PZT (PZT-5H)	Density	7500 kg/m^3
	Elasticity matrix	$\begin{bmatrix} 12.72 & 8.02 & 12.72 & 0 & 0 & 0 \\ 8.02 & 8.47 & 8.47 & 0 & 0 & 0 \\ 12.72 & 8.47 & 11.74 & 0 & 0 & 0 \\ 0 & 0 & 0 & 2.30 & 0 & 0 \\ 0 & 0 & 0 & 0 & 2.30 & 0 \\ 0 & 0 & 0 & 0 & 0 & 2.30 \end{bmatrix}$
	Coupling matrix	$\begin{bmatrix} 0 & 0 & -6.62 & 0 & 0 & -6.62 \\ 0 & 0 & 23.24 & 0 & 17.03 & 0 \\ 17.03 & 0 & 0 & 0 & 0 & 0 \end{bmatrix}$ C/m^2
	Relative permittivity	$\begin{bmatrix} 1704.4 & 1704.4 & 1433.6 \end{bmatrix}$
Si	Density	2329 kg/m^3
	Young's modulus	170 GPa
	Poisson's ratio	0.28
Chamber and channel (water)	Density	997.0479 kg/m^3
	Speed of sound	1480 m/s (at 25 °C)

Table 2
Dimensions of materials.

	Width (μm)	Length (μm)	Height (μm) t
PZT	84	84	3
Si	140	140	10
Chamber	140	140	300
Channel	10	1800	10

Table 3
Values of used coefficients in calculation of acoustic attenuation.

Coefficients	Values	Coefficients	Values
γ	1	ρ_0	1000 kg/m^3
Pr	7	η	1 mPa s
C_R	1480 m/s		

while voltage output is connected to the top of sensing PZT diaphragm in order to obtain the output voltage generated by sound waves. Additionally, the zero charge conditions are applied to four sides of the PZT diaphragm because there does not exist any charge at the sides of PZT diaphragm in the ideal model.

2.3. Finite element modeling of micro-viscometer

The multi-physical simulation of micro-viscometer is conducted using frequency sweep from 3.5 MHz to 5.2 MHz with 1 V applied to the driving PZT diaphragm. The simulation results are plotted in Fig. 6, and this result shows that the output voltage has a maximum value at 4.37 MHz, which is the driving frequency. In other words

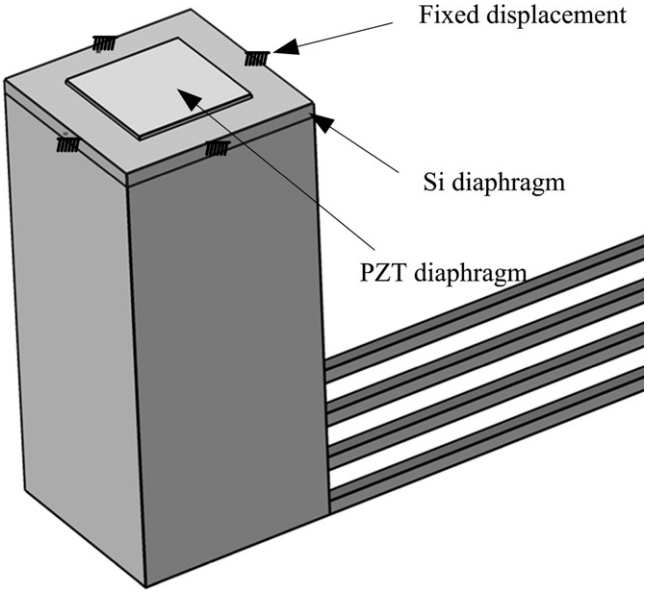

Fig. 4. Boundary conditions of Si diaphragm.

the micro-viscometer has maximum gain and efficiency at 4.37 MHz.

Fig. 7 illustrates the shape of structural displacement of driving and sensing part at the driving frequency, and the difference of the shape between the driving and sensing part comes from the acoustic attenuation effect. This acoustic attenuation effect is confirmed from the simulation results as the acoustic pressure of sensing is smaller than that of driving due to the attenuation of sound waves in microchannels as shown in Fig. 8. Fig. 9 shows that the acoustic pressure distribution reflects the structural displacement of Si and PZT diaphragms, capturing the interaction between acoustical and structural phenomenon. This phenomenon observed as

the near-field effect of sound waves near acoustic-structure boundary of driving part can be explained by the displacement of Si diaphragm not being uniform along the equivalent radius. The near-field effect was not able to be observed in previous simulations [1] which only took in consideration for acoustical phenomenon.

The driving frequency 4.37 MHz of the water-filled simulation result is different from the resonant frequency 5.77 MHz of the vacuum simulation as shown in Fig. 10. This is because of the added mass effect caused by the interaction between the Si diaphragm and internal liquid. The added mass effect on Si diaphragm could not be observed in previously used method which only considered acoustical phenomenon. The capability of multi-physical method to demonstrate the near-field effect of the sound waves and the added mass effect of the Si diaphragm shows that the results of multi-physical method is more accurate than that of the former acoustic method.

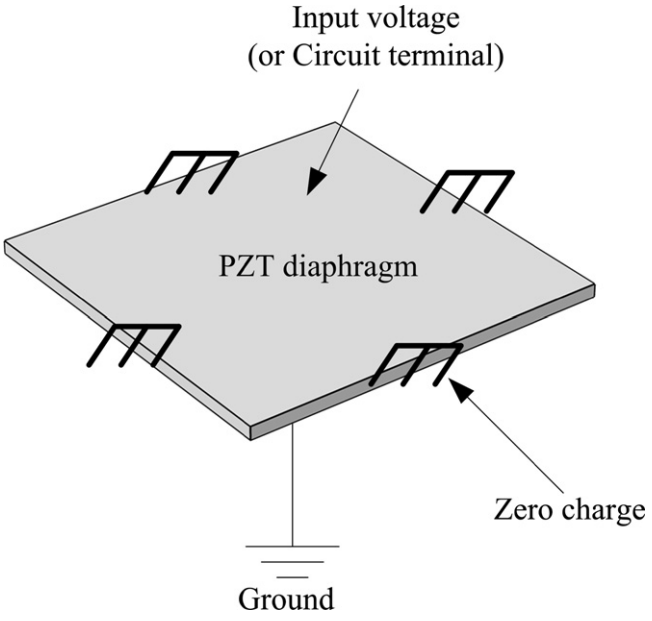

Fig. 5. Boundary conditions of PZT diaphragm.

Table 4
Used dimensions for the optimization of micro-viscometer.

	Radius or width × length(μm)	Height(μm) t
Si (circle)	90	10
Chamber (circle)	90	430
PZT (circle)	r_c (50–70)	3
Channel (rectangle)	30 × 2160	30

3. Optimized design of micro-viscometer

3.1. The design conditions for optimization of micro-viscometer

The micro-viscometer with circular diaphragm type has several advantages compared to the rectangular type. First, theoretical approach of modeling the device for circular type is easier than that of the rectangular, because theoretical models for circular type are found more widely in literature [7–9]. Secondly, the finishing precision is a challenge in MEMS fabrication process for rectangular type, leading to unwanted multi-modes near resonant frequency. Lastly, round type with radius equivalent to that of the rectangular type has higher resonant frequency, leading to reduction of system thickness and material savings in the end. Therefore, in a scope of design improvement, the micro-viscometer with circular diaphragm and circular chambers accordingly is proposed for optimization as shown in Table 4 and Fig. 11.

However, considering the driving frequency, acoustic wave guide, and complexity of the MEMS fabrication process, it is not so simple changing the characteristic dimensions of chambers and Si diaphragms including the thickness of PZT diaphragms. Therefore only the shape and size excluding the thickness of PZT diaphragm are considered as objectives of the optimization. The output voltage of using multi-physical FEM simulation is used for determining optimized dimensions of PZT diaphragms.

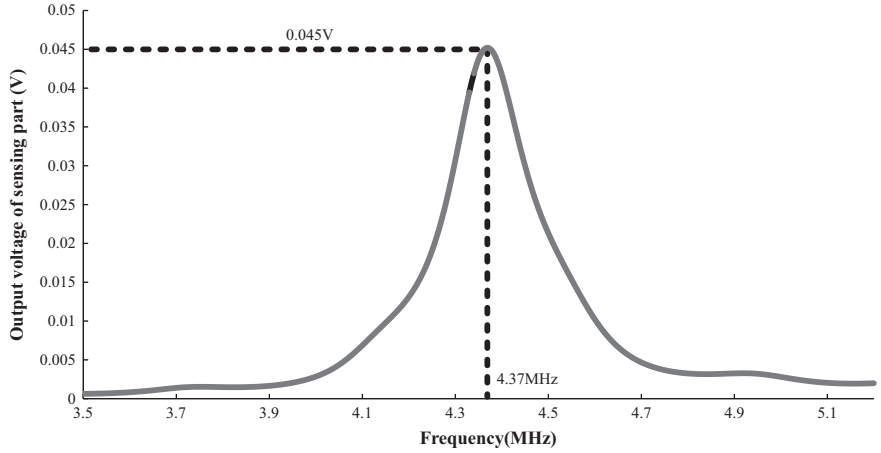

Fig. 6. Output voltage of sensing part in the case of water.

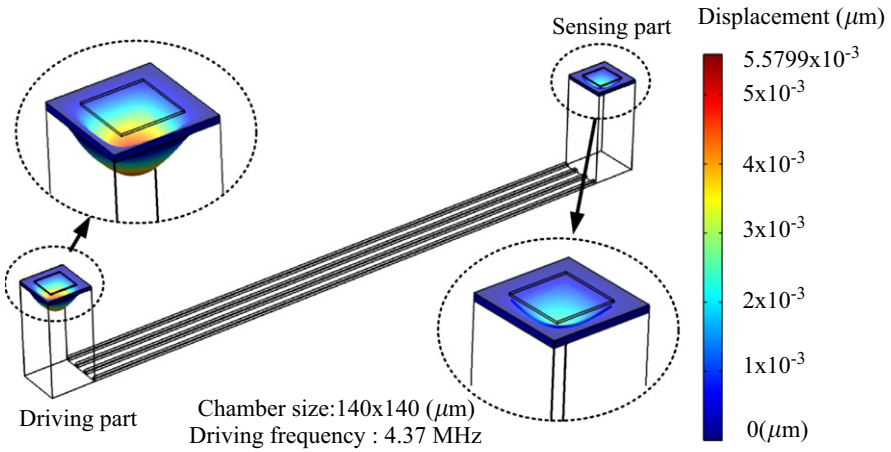

Fig. 7. Structural displacement of PZT–Si diaphragms.

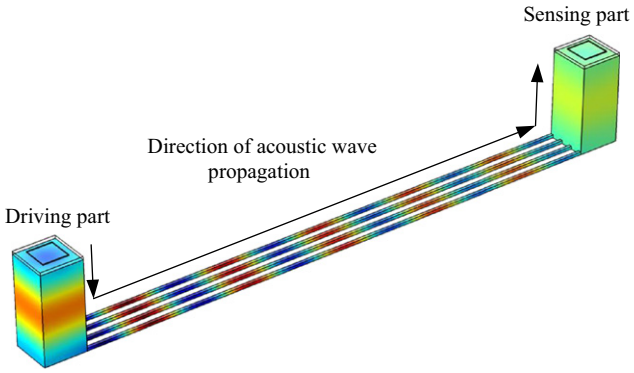

Fig. 8. Acoustic pressures of micro-viscometer.

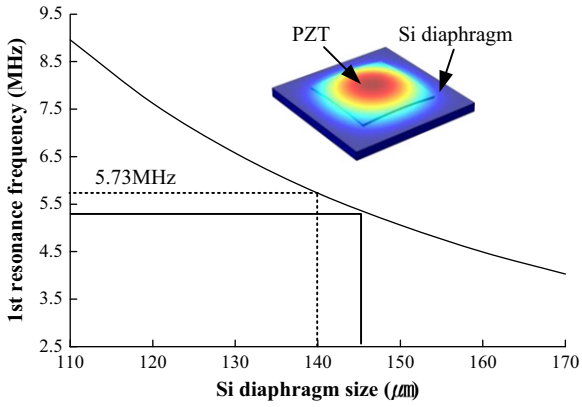

Fig. 10. First resonance frequencies of PZT–Si diaphragm for Si diaphragm size.

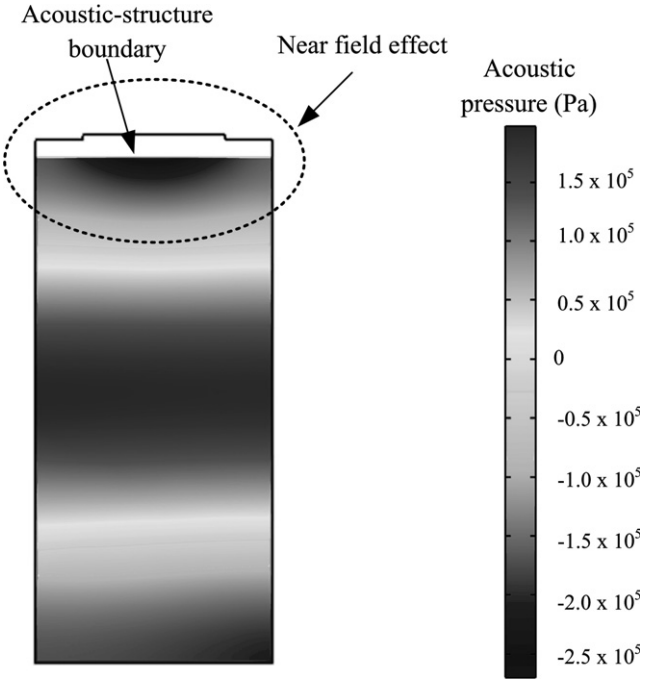

Fig. 9. Acoustic pressure distribution in the chamber of driving part.

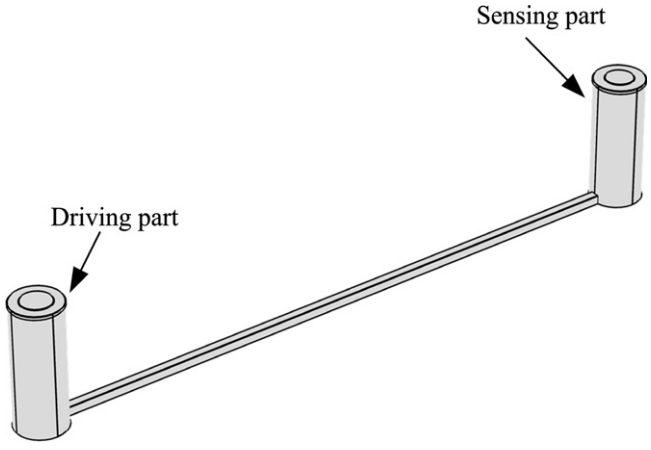

Fig. 11. Micro-viscometer of circular type.

For the optimization of micro-viscometer, round, cross and hexagon shapes are suggested as shown in Fig. 12, where r_c is the characteristic radius which represents the size of each shape ranging from 50 μm to 70 μm. These shapes are only applied to the PZT diaphragm of sensing

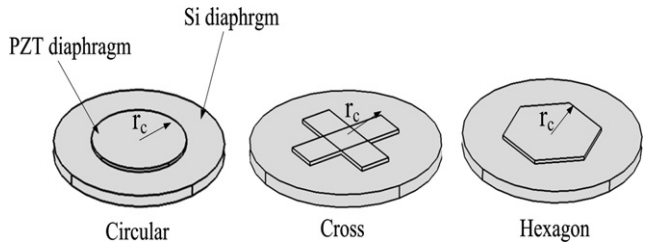

Fig. 12. Considered shapes of PZT diaphragm for the optimization of micro-viscometer.

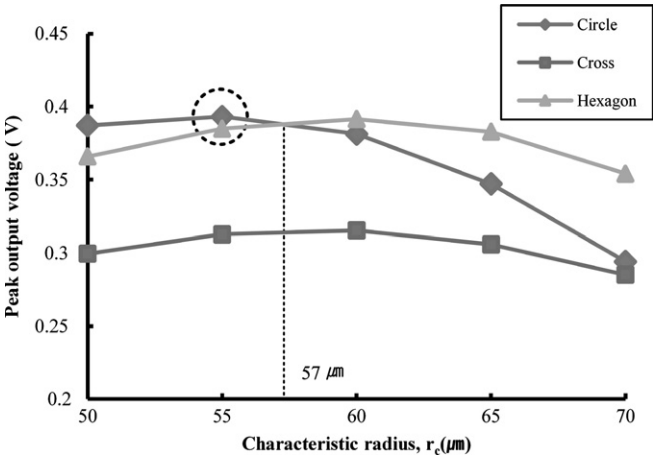

Fig. 13. Comparison of maximum output voltages for shapes of PZT diaphragm.

part in order to maintain equal driving frequency, value of which is dependent on the shape of Si and PZT diaphragm. The dimensions used for the circular micro-viscometer are listed in Table 3, and the 1 V is applied to the PZT diaphragm of driving part.

3.2. The result of optimization

The simulated result for three different shapes of PZT diaphragm is shown in Fig. 13, and each peak value of the output voltage at driving frequency for each shape is plotted against the characteristic radius, r_c. This result shows that PZT diaphragm of circular type with characteristic radius of 55 μm has the highest value. In other words, it means that PZT film of circular type with characteristic radius of 55 μm can be used as the optimal design of micro-viscometer with circular-diaphragm. Meanwhile, in the case of considering characteristic radius of more than 57 μm, it can be seen that choosing hexagonal shape is more optimal than choosing circular shape.

4. Conclusion

The multi-physical approach is proposed for designing a micro-viscometer, and is compared to the previously proposed micro-viscometer. In the multi-physical approach, the near field effect of sound waves and the added mass effects can be observed which was not possible in the only acoustic pressure approach. This result shows that the proposed method can be applied to improve and optimize the design of micro-viscometer. In this research, optimization using the proposed method is carried out for designing a new type micro-viscometer, and fruited to an optimized design of micro-viscometer.

Acknowledgments

This work was supported by the National Research Foundation of Korea (NRF) Grant funded by the Korea government (MEST) (No. 2012-0009458).

This work was also supported by SEED type project (PER12030) funded by the Korea Institute of Industrial Technology.

References

[1] Choi Sungjoon, Moon Wonkyu, Lim Geunbae, A micro-machined viscosity-variation monitoring device using propagation of acoustic waves in microchannels, Journal of Micromechanics and Microengineering 20 (8) (2010) 1–13.
[2] Dragan Damjanovic, Ferroelectric, dielectric and piezoelectric properties of ferroelectric thin films and ceramics, Reports on Progress in Physics 61 (9) (1998) 1267–1324.
[3] IEEE, Standard on Piezoelectrics, ANSI/IEEE Std., 176.
[4] N. Setter, Piezoelectric materials in devices, Ceramics Laboratory, EPFL (2002).
[5] O.C. Zienkiewicz. R.E. Newton, Coupled vibrations of a structure submerged in a compressible fluid, in: Proceedings of the Symposium on Finite Element Techniques. University of Stuttgart, 1969.
[6] Lord Rayleigh, The Theory of Sound, Courier Dover Publications, 1945.
[7] Lawrence E. Kinsler, Austin R. Frey, Alan B. Coppens, James V. Sanders, Fundamental of Acoustics, fourth ed., John Wiley & Sons, Inc., 2000.
[8] T.Blackstock David, Fundamentals of Physical Acousitics, John Wiley & Sons, Inc, 2000.
[9] M.S. Howe, Acoustics of Fluids-structure Interactions, Cambridge Monographs on Mechanics, 1998.